

Article

In-Silico Monte Carlo Simulation Trials for Investigation of V₂O₅ Reinforcement Effect on Ternary Zinc Borate Glasses: Nuclear Radiation Shielding Dynamics

Huseyin O. Tekin^{1,2}, Shams A. M. Issa^{3,4}, Gokhan Kilic⁵, Hesham M. H. Zakaly^{3,6,*}, Mohamed M. Abuzaid¹, Nevzat Tarhan^{2,7}, Khatar Alshammari^{8,9}, Hj Ab Aziz Sidek¹⁰, Khamirul A. Matori¹⁰ and Mohd H. M. Zaid^{10,*}

- ¹ Medical Diagnostic Imaging Department, College of Health Sciences, University of Sharjah, Sharjah 27272, United Arab Emirates; tekin765@gmail.com (H.O.T.); mabdelfatah@sharjah.ac.ae (M.M.A.)
- ² Medical Radiation Research Center (USMERA), Uskudar University, 34672 Istanbul, Turkey; nevzat.tarhan@uskudar.edu.tr
- ³ Physics Department, Faculty of Science, Al-Azhar University, Assiut 71524, Egypt; shams_issa@yahoo.com
- ⁴ Physics Department, Faculty of Science, University of Tabuk, Tabuk 71451, Saudi Arabia
- ⁵ Department of Physics, Eskisehir Osmangazi University, 26040 Eskisehir, Turkey; gkilic@ogu.edu.tr
- ⁶ Institute of Physics and Technology, Ural Federal University, 620000 Ekaterinburg, Russia
- ⁷ NP Istanbul Brain Hospital, 34768 Istanbul, Turkey
- ⁸ Department of Physics, Faculty of Arts and Sciences, Northern Border University, Turaif 75311, Saudi Arabia; alshammari.khatar1@gmail.com
- ⁹ Faculty of Medical Sciences, Newcastle University, Newcastle NE2 4HH, UK
- ¹⁰ Department of Physics, University Putra Malaysia, Serdang 43400, Selangor, Malaysia; sidek@upm.edu.my (H.A.A.S.); khamirul@upm.edu.my (K.A.M.)
- * Correspondence: h.m.zakaly@azhar.edu.eg or h.m.zakaly@gmail.com (H.M.H.Z.); mhmzaid@upm.edu.my (M.H.M.Z.); Tel.: +7-982-648-3682 (H.M.H.Z.)



Citation: Tekin, H.O.; Issa, S.A.M.; Kilic, G.; Zakaly, H.M.H.; Abuzaid, M.M.; Tarhan, N.; Alshammari, K.; Sidek, H.A.A.; Matori, K.A.; Zaid, M.H.M. In-Silico Monte Carlo Simulation Trials for Investigation of V₂O₅ Reinforcement Effect on Ternary Zinc Borate Glasses: Nuclear Radiation Shielding Dynamics. *Materials* **2021**, *14*, 1158.

<https://doi.org/10.3390/ma14051158>

Academic Editor: George Kenanakis

Received: 27 January 2021

Accepted: 24 February 2021

Published: 1 March 2021

Publisher's Note: MDPI stays neutral with regard to jurisdictional claims in published maps and institutional affiliations.



Copyright: © 2021 by the authors. Licensee MDPI, Basel, Switzerland. This article is an open access article distributed under the terms and conditions of the Creative Commons Attribution (CC BY) license (<https://creativecommons.org/licenses/by/4.0/>).

Abstract: In the current study, promising glass composites based on vanadium pentoxide (V₂O₅)-doped zinc borate (ZnB) were investigated in terms of their nuclear-radiation-shielding dynamics. The mass and linear attenuation coefficient, half-value layer, mean free path, tenth-value layer, effective atomic number, exposure-buildup factor, and energy-absorption-buildup factor were deeply simulated by using MCNPX code, Phy-X PSD code, and WinXcom to study the validation of ZBV1, ZBV2, ZBV3, and ZBV4 based on (100-x)(0.6ZnO-0.4B₂O₃)(x)(V₂O₅) (x = 1, 2, 3, 4 mol%) samples against ionizing radiation. The results showed that attenuation competencies of the studied glasses slightly changed while increasing the V₂O₅ content from 1 mol% to 4 mol%. The domination of ZnO concentration in the composition compared to B₂O₃ makes ZnO substitution with V₂O₅ more dominant, leading to a decrease in density. Since density has a significant role in the attenuation of gamma rays, a negative effect was observed. It can be concluded that the aforementioned substitution can negatively affect the shielding competencies of studied glasses.

Keywords: vanadium pentoxide; Monte Carlo simulation; ternary zinc borate; radiation shielding dynamics

1. Introduction

Glasses, which are flexible materials in terms of ease of production and structural variations to production, have vital roles in technology and research [1]. Utilized as the primary raw materials, phosphorus pentoxide, boron oxide, and vanadium pentoxide are the most common compounds in the manufacture of glasses [2–4]. Of these chemicals, B₂O₃ is regarded as the strongest glass former [5–7]. Borate glasses in which B₂O₃ establishes the glass network are mostly used as optical materials because they have low melting points, high transmittance properties, and high thermal stability [8–10]. They are widely used in the processing of dielectric materials, and used in electronic materials. In addition to their use as dielectric components, the presence of transition metal ions in the borate

glass network results in a semiconducting character [11–15]. Transition metals are used in glass science in different contexts because of their complex properties that emerge from several valence states [16]. Zinc oxide/borax glasses are being used in plasma screens and displays for high definition and quality. They are chosen due to their ability to quickly pass energy in dielectric layers and their high transparency [17]. With all of the qualities mentioned above, zinc borate glasses stand out among products for applications that are in doubt. Studies on vanadium have grown recently due to the material's curious optical, electrical, and magnetic properties [18–23]. Though studies on transition-metal-doped glasses can frequently be found in the literature, there are still components, compositions, and properties that have not yet been studied. Despite the broad variety of papers researching transition-metal-doped glasses, many elements, formulations, and properties are not yet researched. On the other hand, analysis suggests that these glasses can be extremely protective against radiation [24–33]. The use of the glass material for radiation shielding is not limited to this kind of glass, but the frequency of experimental studies on the issue has been increasing daily as a hot topic. Any conventional materials such as lead and concrete used in nuclear fields do not possess superior material properties and have some features that can endanger health [34]. Although this report does not say unequivocally that these new shielding materials are an insufficient radiation-shielding material, some organizations such as IAEA have direct incentives for researchers to study new-generation shielding materials. In this case, glasses suit the profile of these kinds of uses. For this aim, the compositions of a group of glasses encoded as ZBV1, ZBV2, ZBV3, and ZBV4 [35] were tested and extensively researched for their capabilities in gamma-radiation attenuation.

In this study, gamma-attenuation properties of the ZnO-B₂O₃-V₂O₅ glass system were investigated in terms of the relationship between substitution-type (i.e., V₂O₅) changes in typical shielding behaviors of glass system. Previously, Kilic [35] investigated the synthesis process and the optical, thermal, and structural properties of four different glasses based on zinc borate containing V₂O₅. His results showed that V₂O₅ enabled the glass-transition temperature of a sample to fall from 553 °C to 531 °C. Moreover, density declined with a rise in the quantity of V₂O₅. Volume improved as the V₂O₅ concentration increased. Compared with the earlier calculation, the refractive index improved. Their large refractive indices suggest that they may be strong optical materials that could be used in optical structures needing a high refractive index. These glasses may be used in many areas of optics, but in some sense are often innovative materials for solar-energy systems due to their semiconducting properties. However, those promising findings are worthy of continuous investigations of aspects such as resistance competencies against gamma rays. In fulfilment of international safety requirements, the value of alternate shielding materials is growing. Therefore, this paper simply focused on examining the interaction between nuclear-radiation-shielding properties in V₂O₅-reinforced ternary zinc borate glasses. This is because of glass materials' potential as attenuator in industrial, medical, and research ionizing-radiation facilities. It is well known that material density has a remarkable impact on gamma-ray-shielding properties [36,37]. Therefore, the importance of traditional shields such as concrete and lead (Pb) is obvious in ionizing-radiation facilities. Since the glasses have been widely reported as alternative shields instead of the aforementioned conventional shields, this study aimed to characterize the material properties of a ZnO-B₂O₃-V₂O₅ system along with its gamma-shielding properties.

M.A. Tunes et al. developed a computational model of a compact pressurized-water nuclear reactor to investigate the use of innovative materials to enhance the biological-shielding effectiveness. They used MCNP and GEM/EVENT codes to simulate the behavior of several materials and the shielding thickness for gamma and neutron radiation [38]. J. Kaewkhao et al. investigated the mass attenuation coefficients and shielding parameters of borate-based glasses involving Bi₂O₃ and BaO. They established that the increment of the mass-attenuation coefficients was a function of the Bi₂O₃, BaO, and PbO contents. Furthermore, the half-value layers of investigated glasses were more favorable than normal concretes and marketable window glasses. These results reflect that the Bi-based glass can

replace Pb in radiation-shielding glass [39]. P. Limkitjaroenporn et al. prepared lead sodium borate glasses via melt-quenching and explored their optical, physical, structural, and gamma-ray-shielding properties. They recorded that the gamma-ray-shielding properties increased with an increase in PbO concentration [40]. K. Kirdsiri et al. measured the radiation-shielding and optical properties of bismuth lead silicate and barium silicate glasses. They observed that total mass-attenuation coefficients of the glasses at 662 keV were enhanced by the increment of Bi₂O₃ and PbO, which elevated the photoelectric absorption in the glass networks [41]. S. Kaewjang et al. fabricated and investigated the (80-x)B₂O₃-10SiO₂-10CaO-xGd₂O₃ (where x = 15, 20, 25, 30, and 35 mol%) for their radiation-shielding, physical, and optical properties. They found that the experimental values of the mass-attenuation coefficients, effective atomic number, and effective electron densities of the glasses increased with the increasing of Gd₂O₃ concentration, and also with the increasing of photon energy from 223 to 662 keV [42]. N. Chanthima et al. investigated the impacts of BaO on the physical properties of zinc borate-based glasses. They recorded that the radiation-shielding parameters were enhanced as a function of BaO, and the decrement of γ -ray energy [43]. K. Boonin et al. synthesized and inspected zinc barium tellurite glasses for their radiation-defense mechanism and structural behavior. They found that the effective atomic number and effective electron density decreased with the increase in γ -ray energies, which is in a good agreement with theoretical values attained using Geant4 and WinXCOM [44]. W. Cheewasukhanont et al. studied the radiation-shielding parameters of bismuth borosilicate-based glasses. The outcomes revealed that the density of the glasses increased with the increase of Bi₂O₃ content, while the particle size did not account for the density. They found that the radiation-shielding parameters of these glasses were enhanced over those for traditional glass windows and for some types of concrete [45]. S. Kaewjaeng et al. prepared and investigated (80-x)B₂O₃:10SiO₂:10CaO:xLa₂O₃ glass (where x = 10, 15, 20, 25, and 30 mol%) for x-ray-shielding, physical, and optical properties. They found that the half-value layer and tenth-value layer of the glass samples tended to decrease when the kVp of an x-ray instrument decreased and La₂O₃ concentrations increased [46]. F. H. ElBatal et al. studied UV-Vis and FTIR absorption spectra of some prepared undoped and NdF₃-doped borophosphate glasses, with varying dopant contents before and after gamma irradiation [47]. H. ElBatal et al. prepared undoped and CuO-doped lithium phosphate, lead phosphate, and zinc phosphate glasses. They measured the UV-VIS and infrared absorption spectra of the prepared samples before and after successive gamma irradiation [48].

This study aims to discuss the potential effects of V₂O₅ substitution on the nuclear-radiation-shielding properties of ZnO-B₂O₃-V₂O₅ glasses. The investigated radiation-attenuation parameters can be ordered as: linear-attenuation coefficients (LACs), mass-attenuation coefficients (MACs), effective electron density (N_{eff}), half-value layer ($T_{1/2}$), exposure buildup factor (EBF), energy-absorption buildup factor (EABF), tenth-value layer (TVL), mean free path (λ), and effective atomic number (Z_{eff}). The obtained outcomes from the current investigation could be useful to understand the direct impact of glass structure, glass density, and replacement type on the radiation-shielding properties of ZnO-B₂O₃-V₂O₅ glasses. In this research report, all the investigated parameters will be discussed in terms of synergistic effect of substitution and changes in the resistance behavior against gamma radiation.

2. Materials and Methods

2.1. Behavioral Changes in ZnO-B₂O₃-V₂O₅ Glasses

Figure 1 shows that the fabricated glasses samples encoded as ZBV1, ZBV2, ZBV3, and ZBV4 based on a (100-x)(0.6ZnO-0.4B₂O₃)(x)(V₂O₅) (x = 1, 2, 3, 4 mol%) system. Glass densities and elemental compositions are presented in Table 1. As can be seen in Table 1, the values for the glass samples gradually declined from 3.392 g/cm³ to 3.329 g/cm³ with rising concentrations of V₂O₅ [35]. On the other hand, the molar volume values rose linearly from 22.910 cm³/mol to 24.289 cm³/mol. Therefore, a smooth decrement

in gamma-ray-attenuation competencies from ZBV1 to ZBV4 can be expected to be a potential consequence.



Figure 1. Studied glass samples [35] and their physical/optical appearances.

Table 1. Chemical compositions and density for glass samples.

Glass Code	mol%				wt%			Density (g/cm ³)
	ZnO	B ₂ O ₃	V ₂ O ₅	B	O	V	Zn	
ZBV1	59.4	39.6	1	0.110149663	0.377094852	0.013108056	0.499647429	3.392
ZBV2	58.8	39.2	2	0.1075809	0.378557769	0.025866008	0.487995323	3.371
ZBV3	58.2	38.8	3	0.105079843	0.379982128	0.038287697	0.476650332	3.339
ZBV4	57.6	38.4	4	0.102643849	0.381369433	0.050386245	0.465600473	3.329

2.2. MCNPX Monte Carlo Simulations

MCNPX general-purpose Monte Carlo code was implemented for gamma-ray-transmission simulations in the current investigation. Accordingly, mass-attenuation coefficients (MACs) of the $(100-x)(0.6\text{ZnO}-0.4\text{B}_2\text{O}_3)(x)(\text{V}_2\text{O}_5)$ ($x = 1, 2, 3, 4$ mol%) glass system was determined. As a first step in the INPUT file, cell cards and surface cards were prepared using elemental mass fractions (wt %) and material densities (Table 1) of ZBV1, ZBV2, ZBV3, and ZBV4 glasses in the 0.015–10 MeV photon-energy range. Next, MAC values obtained from WinXcom [49] and MCNPX [50–52] were compared. The overall MAC values were largely stable regarding variations in incident photon energy. Despite this, smooth numerical differences were reported between WinXcom and the Monte Carlo code (Table 2).

This can be clarified by the form of processes and physics used in the Monte Carlo simulation and random event generator for a radiation-transfer method, whereas WinXcom is a mechanism that utilizes mathematical improvement for direct determination of MACs. It is worth noting that the MCNPX does not explicitly record MAC values. In some instances, some data processing is achieved by looking at performance data. Simulations were created by integrating various details, including information such as input files, cell cards, and source. The glass samples were measured in terms of their elemental mass fractions (weight per unit length), and dimensions (cm). The gamma-ray-emitting systems' total geometry can be seen in Figure 2. In this step, the F4 Tally mesh was directly utilized for detection of attenuated gamma rays. In this tally mesh, the total photon flux in a cell was

determined. Finally, it is worth mentioning that a point radioactive isotope was utilized as a source for incident gamma rays. The simulation process was repeated from 0.015 to 15 MeV for each glass sample. Moreover, a well-known variance-reduction technique known as tracking optimization was utilized. To increase simulation efficiency, neutron and electron tracking were set as off, and only photon tracking was allowed in the cell definition (i.e., IMP: P).

Table 2. Mass-attenuation coefficients (cm²/g) of the studied glass samples obtained using the MCNPX code and Phy-X PSD program.

Energy (MeV)	ZBV1		ZBV2		ZBV3		ZBV4	
	Phy-X PSD	MCNPX						
0.015	41.8266	43.2654	41.3902	42.8624	40.9654	41.2416	40.5516	41.0625
0.02	19.1754	19.6521	18.9681	19.5124	18.7662	18.8126	18.5695	18.7250
0.03	6.2674	6.3124	6.1978	6.3004	6.1300	6.1526	6.0640	6.1236
0.04	2.8399	2.8524	2.8087	2.8324	2.7782	2.7816	2.7485	2.7628
0.05	1.5617	1.5721	1.5451	1.5629	1.5289	1.523	1.5131	1.5321
0.06	0.9800	0.9936	0.9701	0.9824	0.9605	0.972	0.9512	0.9626
0.08	0.5032	0.5092	0.4989	0.5054	0.4947	0.5023	0.4906	0.4926
0.1	0.3261	0.3295	0.3238	0.3286	0.3217	0.3251	0.3195	0.3198
0.15	0.1842	0.1901	0.1835	0.1882	0.1828	0.1862	0.1821	0.1832
0.2	0.1417	0.1421	0.1414	0.141	0.1411	0.1406	0.1408	0.1409
0.3	0.1096	0.111	0.1095	0.1101	0.1094	0.1091	0.1093	0.1089
0.4	0.0946	0.0952	0.0946	0.095	0.0945	0.0947	0.0945	0.0946
0.5	0.0851	0.086	0.085	0.0856	0.085	0.0854	0.085	0.0852
0.6	0.0781	0.0792	0.078	0.079	0.078	0.0782	0.078	0.0781
0.8	0.068	0.0695	0.068	0.0692	0.068	0.0688	0.068	0.0684
1	0.061	0.0624	0.0609	0.0621	0.0609	0.0619	0.0609	0.0612
1.5	0.0496	0.0501	0.0496	0.0499	0.0496	0.0495	0.0496	0.0494
2	0.043	0.0446	0.043	0.0439	0.043	0.0436	0.043	0.0434
3	0.0358	0.0363	0.0358	0.036	0.0358	0.0359	0.0358	0.0356
4	0.032	0.0334	0.032	0.0333	0.0319	0.0331	0.0319	0.0325
5	0.0297	0.0309	0.0297	0.0305	0.0297	0.0302	0.0296	0.0301
6	0.0283	0.0286	0.0282	0.0284	0.0282	0.0283	0.0282	0.0282
8	0.0267	0.0271	0.0267	0.027	0.0267	0.0268	0.0266	0.0267
10	0.026	0.0263	0.026	0.0261	0.026	0.026	0.0259	0.0259
15	0.0257	0.0262	0.0257	0.026	0.0256	0.0259	0.0256	0.0257

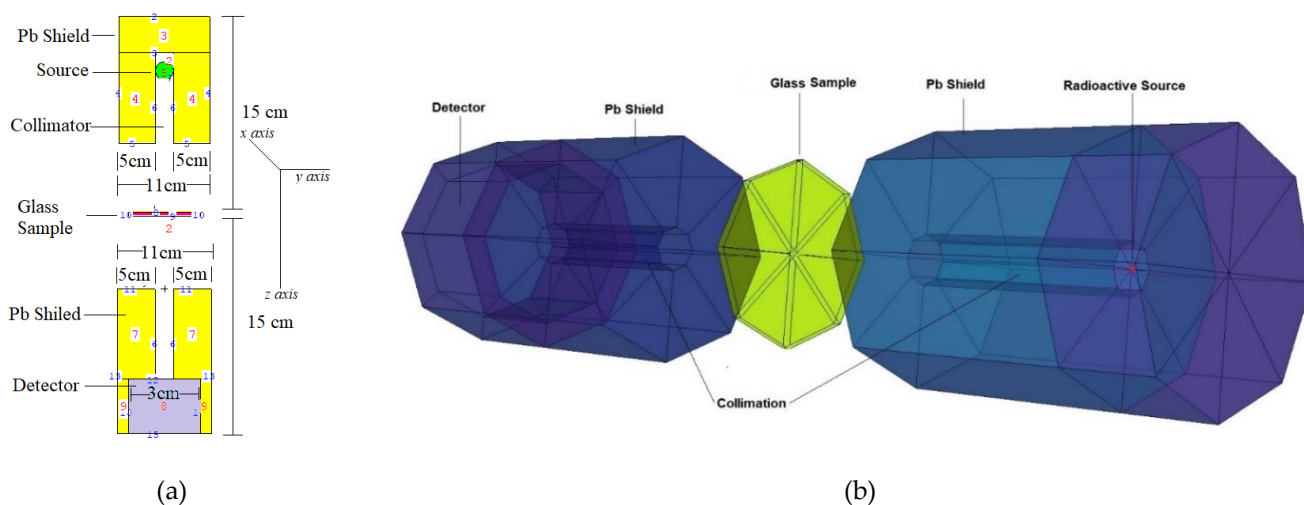


Figure 2. MCNPX simulation setup for gamma-ray-transmission studies: (a) 2D view with dimensions, (b) 3D view of setup obtained from MCNPX Visual Editor.

3. Results and Discussions

To determine the nuclear-radiation-shielding dynamics of V_2O_5 -reinforced ZnO-B $2O_3$ glasses, in silicon Monte Carlo simulation studies were performed. Accordingly, four separate glasses encoded as ZBV1, ZBV2, ZBV3, and ZBV4 based on a $(100-x)(0.6ZnO-0.4B_2O_3)(x)(V_2O_5)$ ($x = 1, 2, 3, 4$ mol. %) glass system was checked for their potentials as possible materials for nuclear-radiation-shielding implementations. In this study, we used Monte Carlo simulations and Phy-X PSD [53] code for determination of shielding parameters. First, linear-attenuation coefficients (LACs) were determined between 0.015–15 MeV gamma photon energy. Figure 3 depicts the variation in the linear attenuation coefficients (μ) against photon energy for all glasses. Figure 3 shows that the influence of the photoelectric effect, Compton scattering, and pair production processes on the LAC was variable depending on the incident energy zones (i.e., low, middle, and high energy). This finding follows as a result of the association of radiation with matter. At low energy values, the LAC is lost due to photo adsorption. Compton scattering accounted for the majority of the energy difference at the mid-energy area, while the lowest LAC was reported in the ZBV4 sample. In other words, the ZBV4 sample with the highest amount of V_2O_5 additive showed the lowest LAC values. In contrast, the ZBV1 sample showed the highest LAC values. In the low-energy region, LAC values were quite similar, whereas in the high-energy region, the differences were slightly higher. The importance of density and direct LAC relationship with density were dominant factors (Figure 3). The mass-attenuation coefficient (MAC) of a material is a specific parameter that can be used in terms of density-independent categorizations of studied shielding materials. Figure 4 illustrates the variations in the mass-attenuation coefficient (μ_m) against incident photon energy for all glasses at 0.015–15 MeV. The chemical structure of the attenuator glass altered the rate of variation of the calculated MAC values. The mathematical analysis of the MAC data show patterns in distinct regions. In the low-energy condition, in which the photoelectric effect is important, the absorption dramatically decreased. Compton-scattering superiority showing the total decrease from the MAC at the mid-energy region. The ZBV1 sample displayed very high atomic concentrations at all incident photon energies. The situation in both the low- and high-energy areas can be clarified by the presence of the highest volume of zinc ($Z = 30$) in the glass structure, since it has a significant atomic number among the utilized composition elements (i.e., B, O, V, Zn).

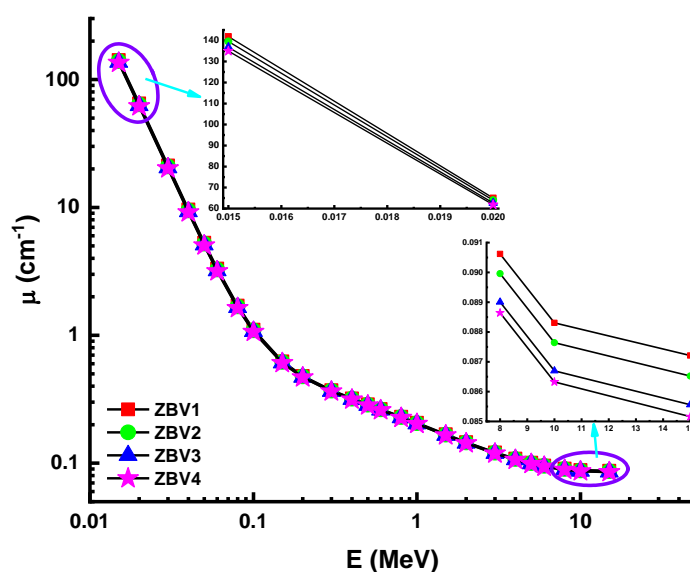


Figure 3. Variation of linear-attenuation coefficient (μ) against photon energy for all glasses.

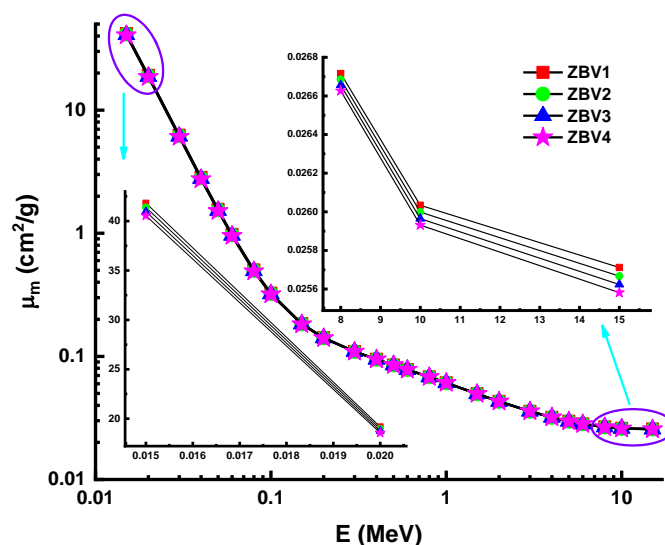


Figure 4. Variation of mass-attenuation coefficient (μ_m) against photon energy for all glasses.

HVL, which stands for “half-value layer” ($T_{1/2}$), is a valuable amount when measuring the thickness of a shielding material in order to minimize gamma rays. So, a smaller HVL may serve as a measure of a material’s capacity to shield incident gamma rays from a primary source. Using the calculated LAC values, the HVLs of the studied glasses were calculated. Figure 5 demonstrates the association between photon energy and $T_{1/2}$ for all glass samples. In the low-energy spectrum, calculations of HVL values were reported smaller. This is a predictable result for shielding in materials that low-intensity gamma rays cannot move through almost completely. To learn more about the efficiency of the studied materials as gamma-ray absorbers, we found it useful to compare them with some of the materials most commonly used as shields against gamma rays. The HVL value for the best glass sample (ZBV4 = 8.13915 cm) at 15 MeV was compared with other shielding materials (lead= 1.08069 cm, ordinary concrete = 13.89992 cm, HSC = 11.63975 cm, ILC = 9.40269 cm, IL = 7.81848 cm, G1 = 15.25284 cm, and G2 = 10.53327 cm) glasses [54,55]. The comparison shows that the ZBV4 glass came third after lead, and with IL outperforming the other shield types. Considering its other distinguishing features, such as lack of toxicity risk and lower weight, this glass is recommended as the ideal choice in many applications that require gamma-ray shields with specific properties.

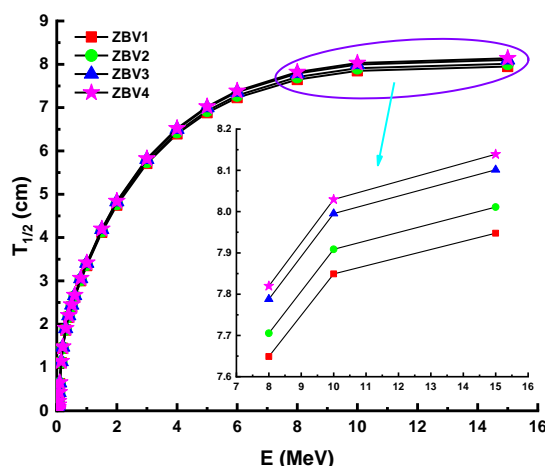


Figure 5. Variation of half-value layer ($T_{1/2}$) against photon energy for all glasses.

However, Figure 5 shows that the HVL values were greater in the mid- as well as the high-energy field. This was attributed to the penetration property of gamma rays and how

it changes with higher energy levels. Considering the direct impact of material densities, which were reported as 3.392 g/cm^3 , 3.371 g/cm^3 , 3.339 g/cm^3 , and 3.329 g/cm^3 for ZBV1, ZBV2, ZBV3, and ZBV4, respectively, the HVL values were changed in similar order. For example, HVL values of $1.109 \text{ cm HVL}_{\text{ZBV1}} < 1.121 \text{ cm HVL}_{\text{ZBV2}} < 1.136 \text{ HVL}_{\text{ZBV3}} < 1.143 \text{ cm HVL}_{\text{ZBV4}}$ were reported at 0.15 MeV. The initial difference in HVL values was 0.034 cm at 0.015 MeV. To confirm the previously mentioned interpretation of the changing trend of HVL values depending on energy region, it is favorable to order those HVL values in the high-energy region. Thus, $7.948 \text{ cm HVL}_{\text{ZBV1}} < 8.011 \text{ cm HVL}_{\text{ZBV2}} < 8.101 \text{ cm HVL}_{\text{ZBV3}} < 8.139 \text{ cm HVL}_{\text{ZBV4}}$ were also reported at 15 MeV. In this case, the difference in HVL values was 0.191 cm at 0.015 MeV. Therefore, one can say that the negative effect of V_2O_5 on HVL values was slightly lower at low energies. Accordingly, the aforementioned reinforcement type negativity can be tolerated at low energy values, considering the positive effects on optical, structural, and thermal properties. The effect of the mean free path (λ) is critical in the capacity of shielding materials to defend against gamma radiation. Glass samples were analyzed in terms of λ values, and details are summarized in Figure 6. The λ values can fluctuate, similar to the shifting patterns in the HVL. The λ values of ZBV1 have been recoded as the minimum in the investigated energy range. Another main element to remember is the tenth-value layer (TVL). The TVL element is another critical criterion to verify the thickness of shields, minimizing gamma rays' strength to 1/10 of their original intensity. The TVLs of the studied samples were calculated, and a graph was drawn showing their importance against incident photon energy (Figure 7). In the lower-energy ranges, the TVL values were lower. Similar to the changing trend in HVL values, TVL values were registered as $3.685 \text{ cm HVL}_{\text{ZBV1}} < 3.722 \text{ cm HVL}_{\text{ZBV2}} < 3.772 \text{ cm HVL}_{\text{ZBV3}} < 3.797 \text{ cm HVL}_{\text{ZBV4}}$ at 0.15 MeV. The effective atomic number (Z_{eff}) of a substance used for gamma-ray exposure regulation would contribute to its photon-attenuation properties. The variation of effective atomic number (Z_{eff}) against photon energy for all glasses is shown in Figure 8.

The Z_{eff} values for ZBV1 glass were the best. For example, a Z_{eff} value of 14.01 was found for the ZBV1 sample at 0.15 MeV. However, the maximum Z_{eff} values recorded for samples were 28.42, 28.30, 28.19, and 28.07 for ZBV1, ZBV2, ZBV3, and ZBV4, respectively. The average photon flux was measured in the detection field by using an F4 tally mesh (Figure 2). Then, an absorption coefficient was used to compensate for a scattering of the radiation. Excess radiation required the cumulative measurement of radiation buildup. The attenuation component was multiplied by the photon's attenuation rate to measure the photon's overall attenuation. The moderator attenuates the penetration of photons of varying intensities such that they both achieve the same reception. In this case, buildup factors can be classified as exposure buildup factor (EBF) and energy-absorption buildup factor (EABF).

In this analysis, a G-P fitting method was utilized for determination of EBF and EABF values. The fitting parameters' calculated numerical values are displayed in Tables 3–6 along with equivalent atomic numbers (Z_{eq}). Figure 9a–d and Figure 10a–d illustrate the measured EBF and EABF values for studied glasses at various mean free paths from 0.6 to 40 mfp. Figures 9 and 10 express the concentration of the different layers of EBF and EABF owing to irradiation by gamma rays. We shall explain the changing trend of EBF and EABF values at different energy values. Due to the photoelectric influence being neglected in regions with large atomic numbers, one may see smooth increments in the first region (Tables 3–6). In addition, the third section of the sample was the most interesting during pair growth due to its absorption processes, which resulted in the decline in its value. Figures 9 and 10 depict the changes in EBF and EABF values of ZBV1, ZBV2, ZBV3, and ZBV4 glass samples for different mean free path (mfp) values (i.e., 0.5, 1, 2, 3, 4, 5, 6, 7, 8, 9, 10, 15, 20, 25, 30, 35, and 40 mfp). These figures demonstrate the reliance of the EBF and EABF values upon the glass structure. The obtained EBF and EABF values showed that ZBV1 had the lowest EBF and EABF levels, and was superior to all other glasses.

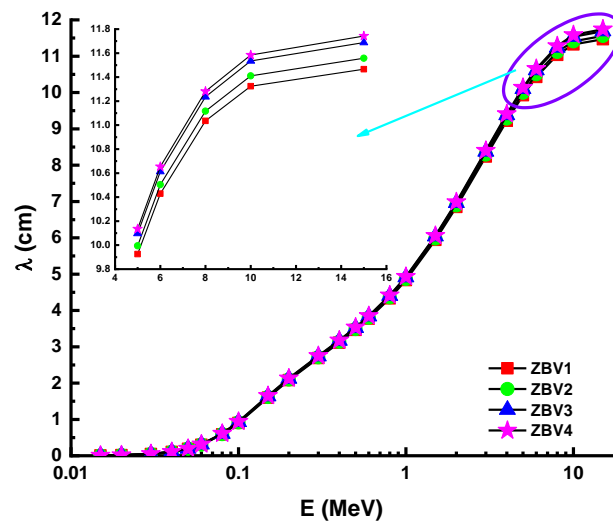


Figure 6. Variation of mean free path (λ) against photon energy for all glasses.

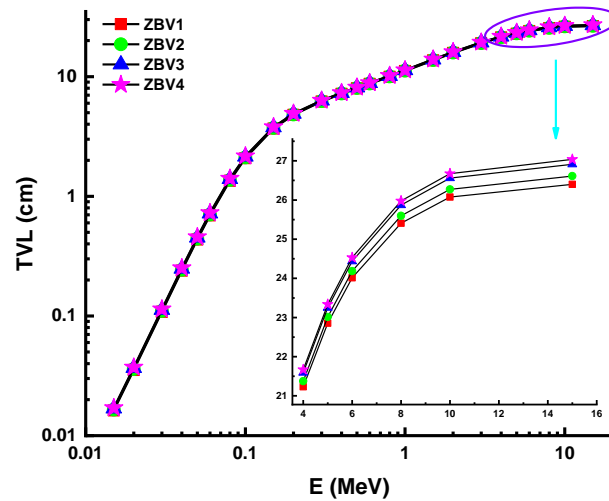


Figure 7. Variation of tenth-value layer (TVL) against photon energy for all glasses.

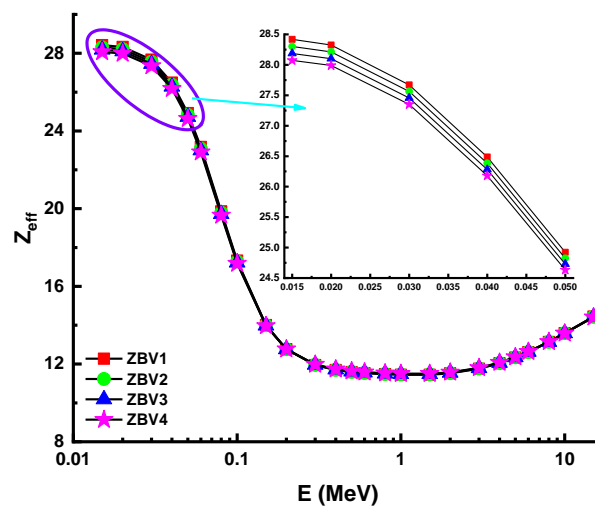


Figure 8. Variation of effective atomic number (Z_{eff}) against photon energy for all glasses.

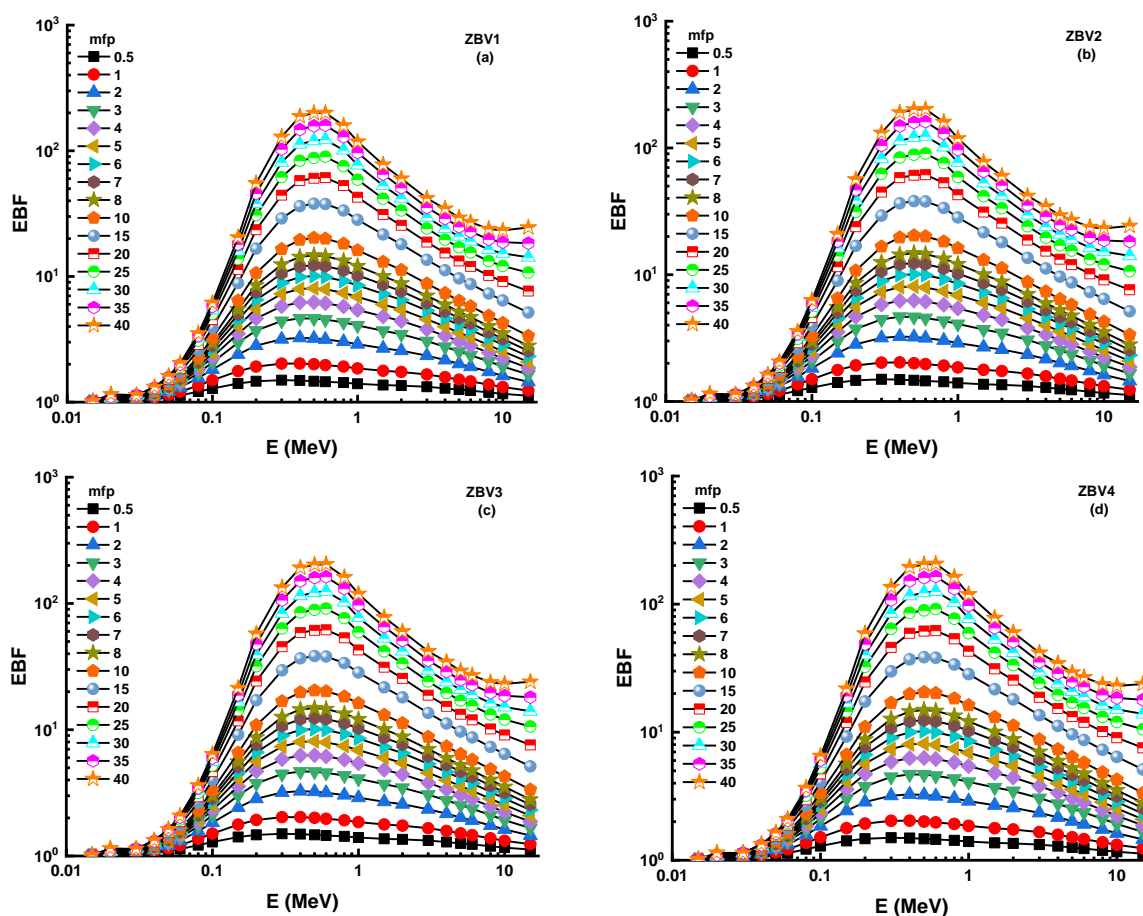


Figure 9. (a–d): Variation of exposure buildup factor (EBF) against photon energy for all glasses.

Figures 11 and 12 show the differing energy-absorption buildup factors (EABF) and exposure buildup factors (EBF) at 0.4 MeV along with 10, 20, 30, and 40 mfp values for all glasses. It can be seen that the ZBV1 sample showed the minimum EBF and EABF values at the studied mfp values. From ZBV1 to ZBV4, EBF and EABF values showed an increasing trend. This can be explained by decreasing gamma-ray-attenuation competencies with a V_2O_5 reinforcement amount from 1 to 4 mol.%. As a last analysis of EBF and EABF values, Figure 13 shows the variations in the energy-absorption buildup factor (EABF) and exposure buildup factor (EBF) against effective atomic number (Z_{eff}) for all glasses at 1 MeV/5 mfp. This is another sign of the synergistic effect of V_2O_5 reinforcement, which caused a decrement in densities of glasses, and in gamma-ray-shielding competencies accordingly. As illustrated in Figure 13, EBF values increased gradually from ZBV1 to ZBV4. This trend was a natural consequence of variations in effective atomic numbers, which was discussed in previous sections.

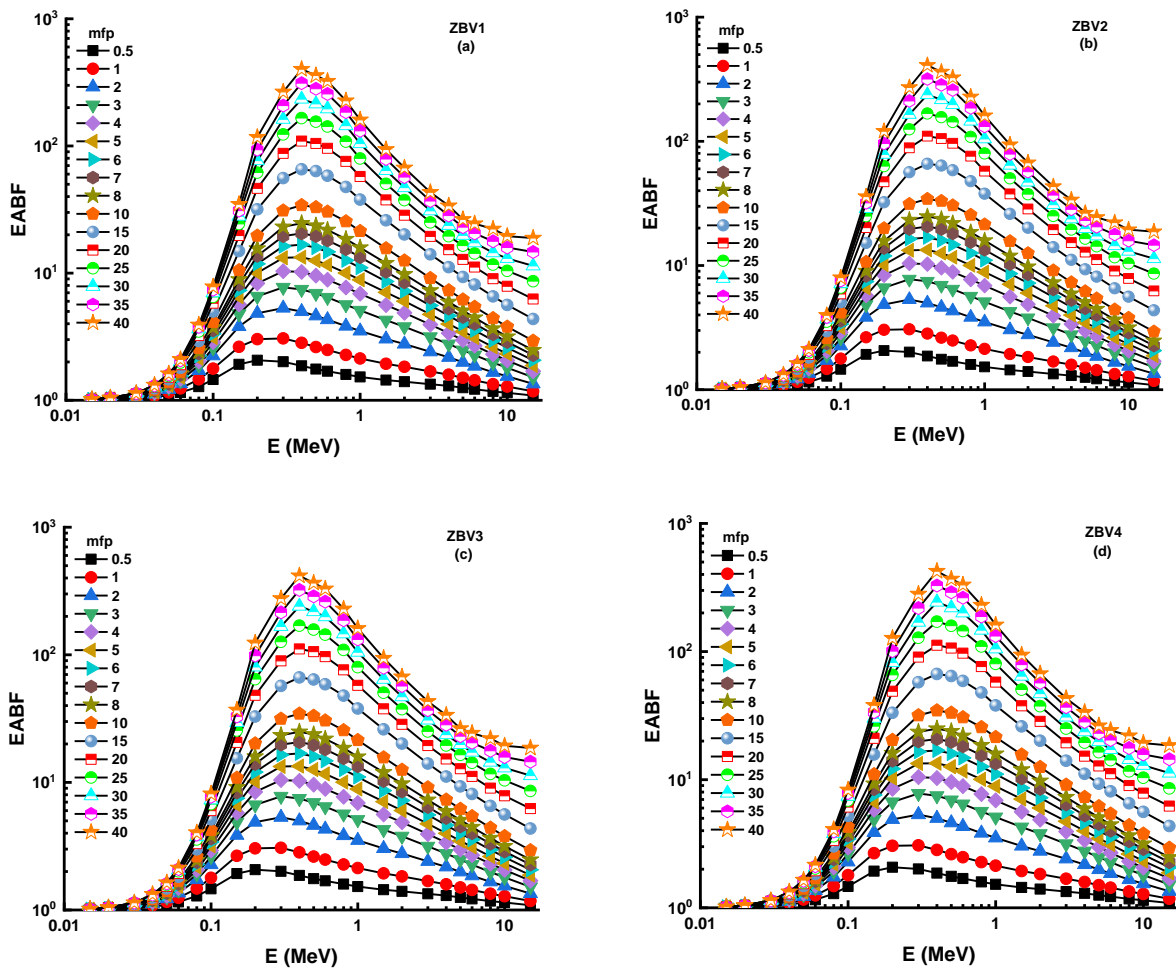


Figure 10. (a–d): Variation of energy-absorption buildup factor (EABF) against photon energy for all glasses.

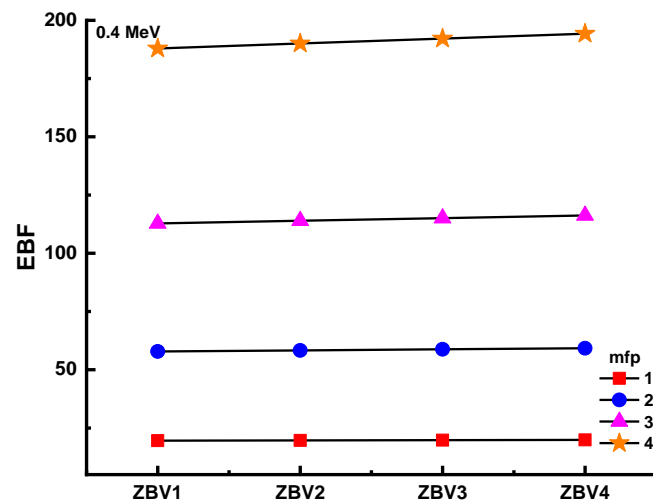


Figure 11. Variation of exposure buildup factor (EBF) against glass compositions.

Table 3. (EBF and EABF) G–P fitting coefficients for the ZBV1 glass sample.

Energy (MeV)	Z_{eq}	G–P Fitting Parameters for EBF					G–P Fitting Parameters for EABF				
		a	b	c	d	X_k	a	b	c	d	X_k
0.015	22.43	0.230	1.006	1.018	0.227	0.223	1.006	1.011	0.217	7.920	−0.223
0.020	22.78	0.398	1.014	0.287	−0.348	0.283	1.014	0.314	−0.236	14.711	0.283
0.030	23.21	0.206	1.041	0.373	−0.231	0.246	1.040	0.337	−0.172	16.253	0.246
0.040	23.47	0.243	1.086	0.347	−0.125	0.238	1.085	0.350	−0.127	13.895	0.238
0.050	23.65	0.225	1.145	0.380	−0.129	0.237	1.154	0.360	−0.134	14.335	0.237
0.060	23.80	0.203	1.211	0.422	−0.113	0.216	1.240	0.398	−0.126	14.724	0.216
0.080	24.00	0.168	1.358	0.502	−0.092	0.174	1.463	0.482	−0.098	15.336	0.174
0.100	24.13	0.129	1.495	0.600	−0.073	0.156	1.772	0.541	−0.094	15.276	0.156
0.150	24.32	0.065	1.763	0.796	−0.043	0.125	2.632	0.657	−0.101	14.589	0.125
0.200	24.43	0.023	1.919	0.960	−0.030	0.061	3.026	0.856	−0.062	13.065	0.061
0.300	24.55	−0.016	2.024	1.131	−0.017	−0.001	3.065	1.086	−0.030	11.983	−0.001
0.400	24.61	−0.031	2.030	1.210	−0.013	−0.029	2.828	1.204	−0.013	14.934	−0.029
0.500	24.65	−0.041	2.000	1.253	−0.008	−0.041	2.624	1.256	−0.008	11.683	−0.041
0.600	24.67	−0.044	1.969	1.264	−0.005	−0.043	2.484	1.266	−0.006	12.436	−0.043
0.800	24.70	−0.042	1.917	1.250	−0.006	−0.044	2.273	1.262	−0.007	9.857	−0.044
1.000	24.70	−0.050	1.853	1.258	0.014	−0.051	2.130	1.265	0.013	17.995	−0.051
1.500	22.35	−0.042	1.777	1.205	0.012	−0.043	1.937	1.210	0.013	15.494	−0.043
2.000	19.86	−0.030	1.738	1.147	0.008	−0.029	1.834	1.144	0.007	17.096	−0.029
3.000	18.94	−0.004	1.658	1.047	−0.011	−0.008	1.685	1.057	−0.006	12.383	−0.008
4.000	18.68	0.008	1.579	1.003	−0.017	0.014	1.590	0.984	−0.023	12.087	0.014
5.000	18.56	0.014	1.510	0.982	−0.021	0.021	1.501	0.962	−0.033	14.147	0.021
6.000	18.48	0.021	1.462	0.962	−0.026	0.027	1.435	0.944	−0.034	12.913	0.027
8.000	18.40	0.032	1.381	0.935	−0.036	0.034	1.339	0.928	−0.034	12.212	0.034
10.000	18.35	0.039	1.319	0.922	−0.042	0.044	1.281	0.903	−0.047	13.903	0.044
15.000	18.31	0.064	1.236	0.866	−0.065	0.035	1.176	0.944	−0.039	14.486	0.035

Table 4. (EBF and EABF) G–P fitting coefficients for the ZBV2 glass sample.

Energy (MeV)	Z_{eq}	G–P Fitting Parameters for EBF					G–P Fitting Parameters for EABF				
		a	b	c	d	X_k	a	b	c	d	X_k
0.015	22.35	0.222	1.006	1.004	0.223	6.425	0.215	1.006	0.998	0.213	7.978
0.020	22.70	0.392	1.014	0.291	−0.341	11.131	0.282	1.014	0.316	−0.234	14.615
0.030	23.13	0.206	1.041	0.373	−0.228	21.387	0.245	1.040	0.338	−0.171	16.167
0.040	23.39	0.242	1.087	0.347	−0.126	12.627	0.238	1.086	0.351	−0.127	13.894
0.050	23.57	0.225	1.147	0.381	−0.129	14.059	0.236	1.156	0.361	−0.134	14.333
0.060	23.71	0.202	1.214	0.423	−0.113	14.198	0.215	1.243	0.399	−0.126	14.725
0.080	23.91	0.168	1.362	0.503	−0.092	14.438	0.173	1.468	0.484	−0.097	15.347
0.100	24.04	0.129	1.500	0.602	−0.073	14.167	0.154	1.780	0.544	−0.094	15.290
0.150	24.23	0.064	1.768	0.798	−0.042	14.004	0.124	2.644	0.661	−0.100	14.567
0.200	24.34	0.022	1.924	0.963	−0.030	13.066	0.060	3.034	0.860	−0.062	13.062
0.300	24.46	−0.016	2.027	1.133	−0.017	11.487	−0.002	3.067	1.090	−0.030	11.952
0.400	24.52	−0.031	2.032	1.212	−0.013	10.506	−0.029	2.829	1.207	−0.012	15.154
0.500	24.56	−0.041	2.002	1.254	−0.008	8.420	−0.041	2.624	1.259	−0.008	11.778
0.600	24.58	−0.044	1.971	1.265	−0.004	11.502	−0.044	2.484	1.267	−0.005	12.591
0.800	24.61	−0.043	1.918	1.252	−0.005	10.254	−0.044	2.273	1.263	−0.007	9.970
1.000	24.61	−0.050	1.854	1.258	0.014	18.992	−0.051	2.130	1.266	0.013	17.965
1.500	22.26	−0.042	1.777	1.205	0.012	15.823	−0.043	1.937	1.210	0.013	15.498
2.000	19.78	−0.030	1.738	1.147	0.008	17.345	−0.029	1.834	1.145	0.007	17.043
3.000	18.88	−0.004	1.658	1.048	−0.011	11.312	−0.008	1.686	1.056	−0.006	12.417
4.000	18.62	0.008	1.579	1.003	−0.017	11.339	0.014	1.590	0.984	−0.022	12.128
5.000	18.50	0.014	1.510	0.982	−0.021	13.395	0.021	1.501	0.963	−0.032	14.300
6.000	18.42	0.021	1.462	0.963	−0.026	13.579	0.027	1.435	0.944	−0.034	12.928
8.000	18.34	0.031	1.381	0.936	−0.035	13.418	0.034	1.339	0.927	−0.034	12.221
10.000	18.30	0.039	1.319	0.921	−0.042	13.453	0.044	1.281	0.905	−0.046	13.904
15.000	18.25	0.066	1.237	0.862	−0.066	13.770	0.035	1.176	0.944	−0.038	14.494

Table 5. (EBF and EABF) G–P fitting coefficients for the ZBV3 glass sample.

Energy (MeV)	Z_{eq}	G–P Fitting Parameters for EBF					G–P Fitting Parameters for EABF				
		a	b	c	d	X_k	a	b	c	d	X_k
0.015	22.27	0.214	1.006	0.991	0.220	6.445	0.207	1.006	0.984	0.210	8.035
0.020	22.62	0.386	1.014	0.295	−0.334	11.124	0.281	1.014	0.318	−0.232	14.520
0.030	23.04	0.207	1.041	0.373	−0.225	21.137	0.245	1.040	0.339	−0.170	16.081
0.040	23.30	0.242	1.088	0.348	−0.126	12.661	0.237	1.087	0.351	−0.127	13.892
0.050	23.48	0.225	1.148	0.381	−0.128	14.061	0.236	1.157	0.361	−0.134	14.330
0.060	23.62	0.202	1.216	0.424	−0.113	14.199	0.215	1.246	0.401	−0.125	14.726
0.080	23.82	0.167	1.366	0.505	−0.092	14.437	0.173	1.474	0.486	−0.097	15.357
0.100	23.95	0.128	1.505	0.604	−0.072	14.169	0.153	1.789	0.547	−0.093	15.303
0.150	24.14	0.063	1.774	0.801	−0.042	13.998	0.123	2.655	0.665	−0.099	14.546
0.200	24.25	0.022	1.928	0.966	−0.030	13.057	0.059	3.042	0.863	−0.061	13.059
0.300	24.37	−0.016	2.030	1.135	−0.017	11.464	−0.003	3.069	1.093	−0.030	11.921
0.400	24.43	−0.032	2.035	1.214	−0.013	10.492	−0.030	2.829	1.210	−0.012	15.370
0.500	24.47	−0.041	2.004	1.255	−0.008	8.425	−0.042	2.623	1.261	−0.007	11.871
0.600	24.49	−0.044	1.972	1.267	−0.004	11.717	−0.044	2.484	1.269	−0.005	12.743
0.800	24.52	−0.043	1.919	1.253	−0.005	10.408	−0.045	2.273	1.265	−0.006	10.080
1.000	24.52	−0.050	1.855	1.259	0.014	18.959	−0.051	2.130	1.267	0.013	17.936
1.500	22.17	−0.042	1.778	1.205	0.012	15.821	−0.043	1.937	1.211	0.013	15.502
2.000	19.71	−0.030	1.739	1.147	0.007	17.271	−0.029	1.834	1.145	0.007	16.991
3.000	18.82	−0.004	1.658	1.048	−0.010	11.333	−0.008	1.686	1.056	−0.006	12.451
4.000	18.56	0.008	1.579	1.003	−0.017	11.305	0.014	1.590	0.984	−0.022	12.169
5.000	18.44	0.014	1.511	0.982	−0.021	13.393	0.020	1.501	0.964	−0.032	14.450
6.000	18.37	0.020	1.462	0.963	−0.025	13.595	0.027	1.435	0.944	−0.034	12.943
8.000	18.29	0.031	1.381	0.936	−0.035	13.413	0.034	1.340	0.927	−0.034	12.231
10.000	18.24	0.039	1.320	0.921	−0.042	13.447	0.043	1.281	0.906	−0.046	13.905
15.000	18.20	0.067	1.239	0.858	−0.067	13.791	0.034	1.176	0.945	−0.038	14.502

Table 6. (EBF and EABF) G–P fitting coefficients for the ZBV4 glass sample.

Energy (MeV)	Z_{eq}	G–P Fitting Parameters for EBF					G–P Fitting Parameters for EABF				
		a	b	c	d	X_k	a	b	c	d	X_k
0.015	22.19	0.206	1.006	0.978	0.217	6.465	0.198	1.006	0.971	0.207	8.091
0.020	22.54	0.380	1.014	0.300	−0.326	11.117	0.280	1.014	0.319	−0.231	14.426
0.030	22.96	0.207	1.042	0.373	−0.223	20.895	0.245	1.041	0.339	−0.170	15.999
0.040	23.22	0.242	1.089	0.348	−0.126	12.695	0.237	1.088	0.352	−0.127	13.891
0.050	23.40	0.224	1.150	0.382	−0.128	14.062	0.236	1.159	0.362	−0.134	14.328
0.060	23.54	0.202	1.219	0.424	−0.113	14.200	0.214	1.249	0.402	−0.125	14.727
0.080	23.73	0.167	1.370	0.506	−0.091	14.435	0.172	1.479	0.488	−0.096	15.367
0.100	23.86	0.127	1.510	0.606	−0.072	14.172	0.152	1.797	0.550	−0.093	15.317
0.150	24.05	0.063	1.779	0.804	−0.042	13.993	0.121	2.666	0.669	−0.098	14.525
0.200	24.16	0.021	1.933	0.969	−0.029	13.049	0.058	3.050	0.867	−0.061	13.056
0.300	24.28	−0.017	2.033	1.137	−0.016	11.443	−0.004	3.071	1.096	−0.029	11.891
0.400	24.35	−0.032	2.037	1.215	−0.013	10.479	−0.030	2.829	1.212	−0.011	15.580
0.500	24.38	−0.041	2.006	1.256	−0.008	8.430	−0.042	2.623	1.263	−0.007	11.961
0.600	24.40	−0.045	1.974	1.268	−0.004	11.927	−0.045	2.484	1.271	−0.004	12.891
0.800	24.43	−0.043	1.920	1.254	−0.004	10.559	−0.045	2.272	1.266	−0.006	10.188
1.000	24.43	−0.050	1.856	1.259	0.014	18.927	−0.051	2.130	1.267	0.013	17.908
1.500	22.08	−0.042	1.779	1.205	0.012	15.819	−0.043	1.937	1.211	0.013	15.506
2.000	19.64	−0.030	1.739	1.147	0.007	17.198	−0.029	1.834	1.145	0.007	16.941
3.000	18.76	−0.004	1.658	1.048	−0.010	11.354	−0.008	1.687	1.056	−0.006	12.484
4.000	18.50	0.008	1.579	1.003	−0.016	11.271	0.014	1.590	0.984	−0.022	12.208
5.000	18.39	0.014	1.511	0.981	−0.021	13.392	0.020	1.501	0.965	−0.032	14.597
6.000	18.31	0.020	1.462	0.963	−0.025	13.610	0.027	1.435	0.944	−0.034	12.957
8.000	18.23	0.031	1.380	0.936	−0.035	13.409	0.035	1.340	0.926	−0.034	12.240
10.000	18.19	0.039	1.320	0.921	−0.042	13.441	0.043	1.281	0.907	−0.045	13.906
15.000	18.15	0.068	1.240	0.854	−0.068	13.812	0.034	1.176	0.946	−0.037	14.509

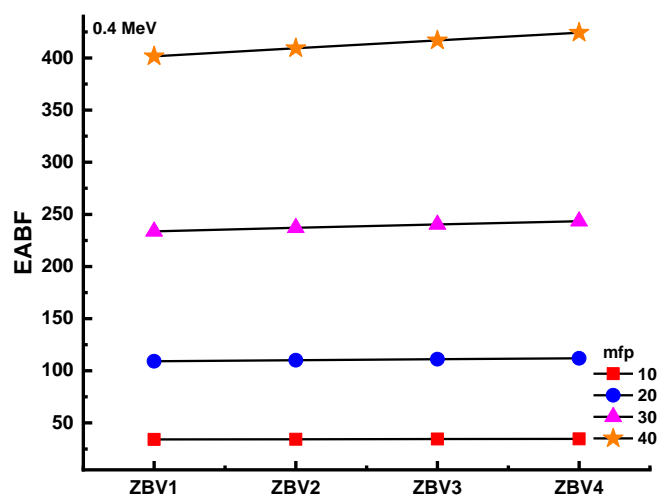


Figure 12. Variation of energy-absorption buildup factor (EABF) against glass compositions.

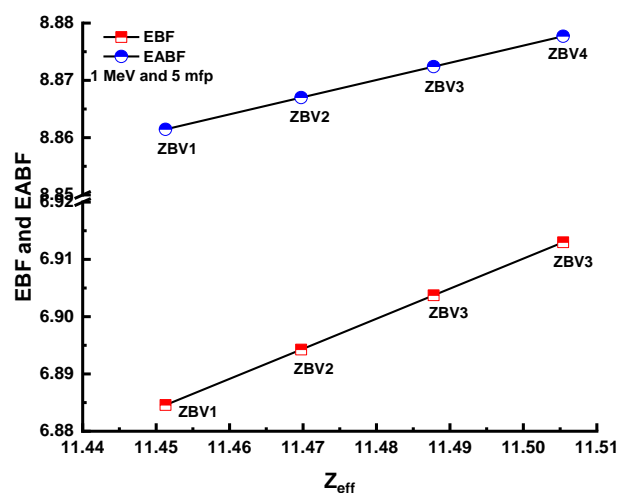


Figure 13. Variation of energy-absorption buildup factor (EABF) and exposure buildup factor (EBF) against effective atomic number (Z_{eff}) for all glasses.

4. Conclusions

Glasses doped with transition-metal oxides were reported to show semiconducting properties in many experimental data due to their multivalent states. Furthermore, boron oxide-based glasses are preferred since they can be synthesized easily, and due to their many characteristic optical and thermal properties. In fact, since zinc borate oxide glasses have a broad spectrum of formation range, they have been the hosts for dopant many times. Zinc borate glasses with a high ZnO ratio were doped with vanadium oxide at varying ratios and constituted the study samples. Increasing the amount of V_2O_5 within the structure resulted in a negative effect, contrary to what was expected in a previous study, and this was valid for the radiation properties observed in this study. V_2O_5 replaced B_2O_3 and ZnO. Though vanadium is an element that is heavier than boron, it is lighter than zinc. The domination of ZnO concentration in the composition compared to B_2O_3 made the ZnO substitution with V_2O_5 more dominant, leading to a decrease in density. Since density has a significant role in data obtained from radiation calculations, the negative effect was observed. The first outcome can be associated with the relationship of density variation and gamma-ray-attenuation properties, since the density values of the samples were changed with the V_2O_5 additive. Considering the obtained results for gamma-ray-attenuation properties, it can be concluded that V_2O_5 reinforcement had an adverse impact against gamma rays. This situation was obtained for all the gamma-ray-attenuation properties

such as LAC, MAC, HVL, TVL, mfp, Z_{eff} , EBF, and EABF. Some of the numerical values were discussed in previous sections. Among the investigated glasses, ZBV1 was reported to have the highest gamma-ray-attenuation properties. Therefore, it can be said that ZBV1 would attenuate incident gamma rays at the maximum level. It can be concluded that some other investigations, such as on mechanical properties acquired upon utilization, should be performed.

Author Contributions: Conceptualization, G.K., H.M.H.Z. and M.H.M.Z.; methodology, G.K.; software, H.O.T., S.A.M.I., H.M.H.Z.; validation, H.O.T., S.A.M.I., H.M.H.Z., H.A.A.S., M.M.A., K.A., K.A.M.; formal analysis, G.K., N.T., H.M.H.Z., M.M.A., M.H.M.Z.; investigation, H.O.T., S.A.M.I., G.K., K.A., H.M.H.Z.; resources, G.K., S.A.M.I.; data curation, H.O.T., H.M.H.Z.; writing—original draft preparation, H.M.H.Z., M.M.A., M.H.M.Z.; writing—review and editing, H.O.T., S.A.M.I., N.T., K.A., H.A.A.S., K.A.M.; visualization, H.M.H.Z.; supervision, G.K., H.M.H.Z., M.H.M.Z.; project administration, H.M.H.Z., M.M.A., M.H.M.Z.; funding acquisition, H.A.A.S., M.H.M.Z. All authors have read and agreed to the published version of the manuscript.

Funding: This research received no external funding.

Institutional Review Board Statement: Not applicable.

Informed Consent Statement: Not applicable.

Data Availability Statement: Not applicable.

Conflicts of Interest: The authors declare no conflict of interest.

References

- Kilic, G.I.U. Synthesis of Nb⁵⁺ Doped Zinc Borate Glasses for Optoelectronic Applications and Determination of Optical, Thermal and Structural Properties. *J. Adv. Res. Nat. Appl. Sci.* **2020**, *6*, 66–80.
- El-Falaky, G.; Gaafar, M.; El-Aal, N.A. Ultrasonic relaxation in Zinc-Borate glasses. *Curr. Appl. Phys.* **2012**, *12*, 589–596. [[CrossRef](#)]
- Wu, J.; Xie, C.; Hu, J.; Zeng, D.; Wang, A. Microstructure and electrical characteristics of ZnO–B₂O₃–PbO–V₂O₅–MnO₂ ceramics prepared from ZnO nanopowders. *J. Eur. Ceram. Soc.* **2004**, *24*, 3635–3641. [[CrossRef](#)]
- Kilic, G.; Ilik, E.; Issever, U.G.; Peker, M. The effect of B₂O₃/CdO substitution on structural, thermal, and optical properties of new black PVB/Cd semiconducting oxide glasses. *Appl. Phys. A* **2020**, *126*, 1–12. [[CrossRef](#)]
- Kilic, G.; Aral, E. Determination of optical band gaps and structural properties of Cu²⁺ Doped B₂O₃–Na₂O–Al₂O₃–V₂O₅ Glasses. *Gazi Univ. J. Sci.* **2009**, *22*, 129–139.
- Rao, R.B.; Veeraiah, N.; Nalluri, V. Study on some physical properties of Li₂O–MO–B₂O₃: V₂O₅ glasses. *Phys. B Condens. Matter* **2004**, *348*, 256–271. [[CrossRef](#)]
- Ilik, E.; Kilic, G.; Issever, U.G. Synthesis of novel AgO-doped vanadium–borophosphate semiconducting glasses and investigation of their optical, structural, and thermal properties. *J. Mater. Sci. Mater. Electron.* **2020**, *31*, 8986–8995. [[CrossRef](#)]
- El-Batal, H.A.R.; Ezz-El-Din, F.M. Interaction of gamma-rays with Some Alkali-Alkaline-Earth Borate Glasses Containing Chromium. *J. Am. Ceram. Soc.* **1993**, *76*, 523–529. [[CrossRef](#)]
- Marltan, W.; Rao, P.V.; Tekin, H.; Sayyed, M.; Klement, R.; Galusek, D.; Lakshminarayana, G.; Prasad, P.S.; Veeraiah, N. Analysis of red mud doped Bi₂O₃–B₂O₃–BaO glasses for application as glass solder in radiation shield repair using MCNPX simulation. *Ceram. Int.* **2019**, *45*, 7619–7626. [[CrossRef](#)]
- Kilic, G.; Ilik, E.; Mahmoud, K.; El-Mallawany, R.; El-Agawany, F.; Rammah, Y. Novel zinc vanadyl boro-phosphate glasses: ZnO–V₂O₅–P₂O₅–B₂O₃: Physical, thermal, and nuclear radiation shielding properties. *Ceram. Int.* **2020**, *46*, 19318–19327. [[CrossRef](#)]
- He, F.; Wang, J.; Deng, D. Effect of Bi₂O₃ on structure and wetting studies of Bi₂O₃–ZnO–B₂O₃ glasses. *J. Alloys Compd.* **2011**, *509*, 6332–6336. [[CrossRef](#)]
- Li, S.; Chen, P.; Li, Y. Structural and physical properties in the system ZnO–B₂O₃–P₂O₅–RnOm. *Phys. B Condens. Matter* **2010**, *405*, 4845–4850. [[CrossRef](#)]
- Aleksandrov, L.A.; Komatsu, T.; Iordanova, R.; Dimitriev, Y. Structure study of MoO₃–ZnO–B₂O₃ glasses by Raman spectroscopy and formation of α -ZnMoO₄ nanocrystals. *Opt. Mater.* **2011**, *33*, 839–845. [[CrossRef](#)]
- Bale, S.; Rahman, S. Electrical conductivity studies of Bi₂O₃–Li₂O–ZnO–B₂O₃ glasses. *Mater. Res. Bull.* **2012**, *47*, 1153–1157. [[CrossRef](#)]
- Ozturk, S.; Ilik, E.; Kilic, G.; Issever, U.G. Ta₂O₅-doped zinc-borate glasses: Physical, structural, optical, thermal, and radiation shielding properties. *Appl. Phys. A* **2020**, *126*, 1–16. [[CrossRef](#)]
- Tekin, H.O.; Kassab, L.R.P.; Issa, S.A.M.; Dias da Silva Bordon, C.; Al-Buriah, M.S.; de Oliveira Pereira Delboni, F.; Kilic, G.; Magalhaes, E.S. Structural and physical characterization study on synthesized tellurite (TeO₂) and germanate (GeO₂) glass shields using XRD, Raman spectroscopy, FLUKA and PHITS. *Opt. Mater.* **2020**, *110*. [[CrossRef](#)]

17. Kilic, G.; Issa, S.; Ilik, E.; Kilicoglu, O.; Tekin, H. A journey for exploration of Eu_2O_3 reinforcement effect on zinc-borate glasses: Synthesis, optical, physical and nuclear radiation shielding properties. *Ceram. Int.* **2021**, *47*, 2572–2583. [[CrossRef](#)]
18. İşsever, U.G.; Kilic, G.; Peker, M.; Ünalı, T.; Aybek, A. Şenol Effect of low ratio V^{5+} doping on structural and optical properties of borotellurite semiconducting oxide glasses. *J. Mater. Sci. Mater. Electron.* **2019**, *30*, 15156–15167. [[CrossRef](#)]
19. Dimitrov, V.; Dimitriev, Y.; Montenero, A. IR spectra and structure of $\text{V}_2\text{O}_5\text{GeO}_2\text{Bi}_2\text{O}_3$ glasses. *J. Non. Cryst. Solids* **1994**, *180*, 51–57. [[CrossRef](#)]
20. Ravikumar, R.; Reddy, V.R.; Chandrasekhar, A.; Reddy, B.; Reddy, Y.; Rao, P. Tetragonal site of transition metal ions doped sodium phosphate glasses. *J. Alloys Compd.* **2002**, *337*, 272–276. [[CrossRef](#)]
21. Hirashima, H.; Arai, D.; Yoshida, T. Electrical Conductivity of $\text{PbO-P}_2\text{O}_5\text{-V}_2\text{O}_5$ Glasses. *J. Am. Ceram. Soc.* **1985**, *68*, 486–489. [[CrossRef](#)]
22. Srinivas, B.; Hameed, A.; Shareefuddin, M.; Chary, M.N. EPR and optical studies of $\text{BaO-TeO}_2\text{-TiO}_2\text{-B}_2\text{O}_3$ glasses containing V^{4+} and Cu^{2+} transitional metal ion. In *Proceedings of the Materials Today: Proceedings*; Elsevier Ltd: Amsterdam, the Netherlands, 2015; Volume 2, pp. 1915–1922.
23. Nagaraja, N.; Sankarappa, T.; Kumar, M.P. Electrical conductivity studies in single and mixed alkali doped cobalt-borate glasses. *J. Non-Crystalline Solids* **2008**, *354*, 1503–1508. [[CrossRef](#)]
24. Hemeda, O.; Eid, M.; Sharshar, T.; Ellabany, H.; Henaish, A. Synthesis of nanometer-sized PbZr Ti1-O3 for gamma-ray attenuation. *J. Phys. Chem. Solids* **2021**, *148*, 109688. [[CrossRef](#)]
25. Sallam, O.; Madbouly, A.; Elalaily, N.; Ezz-Eldin, F. Physical properties and radiation shielding parameters of bismuth borate glasses doped transition metals. *J. Alloys Compd.* **2020**, *843*, 156056. [[CrossRef](#)]
26. Henaish, A.M.A.; Mostafa, M.; Salem, B.I.; Zakaly, H.M.H.; Issa, S.A.M.; Weinstein, I.A.; Hemeda, O.M. Spectral, electrical, magnetic and radiation shielding studies of Mg-doped Ni-Cu-Zn nanoferrites. *J. Mater. Sci. Mater. Electron.* **2020**, 1–13. [[CrossRef](#)]
27. Abouhaswa, A.; Zakaly, H.M.; Issa, S.A.; Rashad, M.; Pyshkina, M.; Tekin, H.; El-Mallawany, R.; Mostafa, M.Y. Synthesis, physical, optical, mechanical, and radiation attenuation properties of $\text{TiO}_2\text{-Na}_2\text{O-Bi}_2\text{O}_3\text{-B}_2\text{O}_3$ glasses. *Ceram. Int.* **2021**, *47*, 185–204. [[CrossRef](#)]
28. Elazaka, A.; Zakaly, H.M.; Issa, S.A.; Rashad, M.; Tekin, H.; Saudi, H.; Gillette, V.; Erguzel, T.; Mostafa, A. New approach to removal of hazardous Bypass Cement Dust (BCD) from the environment: $20\text{Na}_2\text{O-}20\text{BaCl}_2\text{-(}60-x\text{)B}_2\text{O}_3\text{-(}x\text{)BCD}$ glass system and Optical, mechanical, structural and nuclear radiation shielding competences. *J. Hazard. Mater.* **2021**, *403*, 123738. [[CrossRef](#)]
29. Zakaly, H.M.; Saudi, H.; Issa, S.A.; Rashad, M.; Elazaka, A.; Tekin, H.; Saddeek, Y. Alteration of optical, structural, mechanical durability and nuclear radiation attenuation properties of barium borosilicate glasses through BaO reinforcement: Experimental and numerical analyses. *Ceram. Int.* **2021**, *47*, 5587–5596. [[CrossRef](#)]
30. Zakaly, H.M.; Abouhaswa, A.; Issa, S.A.M.; Mostafa, M.Y.A.; Pyshkina, M.; El-Mallawany, R. Optical and nuclear radiation shielding properties of zinc borate glasses doped with lanthanum oxide. *J. Non-Crystalline Solids* **2020**, *543*, 120151. [[CrossRef](#)]
31. Mostafa, A.; Zakaly, H.M.; Pyshkina, M.; Issa, S.A.; Tekin, H.; Sidek, H.; Matori, K.; Zaid, M. Multi-objective optimization strategies for radiation shielding performance of BZBB glasses using Bi_2O_3 : A FLUKA Monte Carlo code calculations. *J. Mater. Res. Technol.* **2020**, *9*, 12335–12345. [[CrossRef](#)]
32. Saudi, H.A.; El Kameesy, S.U. Effect of barium addition and plasma nitriding treatment on chemical and physical properties of Al, Pb borate glass system as a developed radiation shield. In *Proceedings of the Journal of Physics: Conference Series*; IOP Publishing: Luxor, Egypt, 2019; Volume 1253, p. 012033.
33. Singh, K.; Singh, H.; Sharma, G.; Gerward, L.; Khanna, A.; Kumar, R.; Nathuram, R.; Sahota, H.S. Gamma-ray shielding properties of $\text{CaO-SrO-B}_2\text{O}_3$ glasses. *Radiat. Phys. Chem.* **2005**, *72*, 225–228. [[CrossRef](#)]
34. Kaplan, M.F. *Concrete Radiation Shielding*; John Wiley & Sons, Inc: New York, NY, USA, 1989.
35. Kiliç, G. Synthesis and Optical, Thermal, Structural Investigation of Zinc-Borate Glasses Containing V_2O_5 . *Adiyaman Univ. J. Sci.* **2020**, *10*, 307–325. [[CrossRef](#)]
36. Issa, S.A. Effective atomic number and mass attenuation coefficient of $\text{PbO-BaO-B}_2\text{O}_3$ glass system. *Radiat. Phys. Chem.* **2016**, *120*, 33–37. [[CrossRef](#)]
37. Yasmin, S.; Barua, B.S.; Khandaker, M.U.; Chowdhury, F.-U.-Z.; Rashid, A.; Bradley, D.A.; Olatunji, M.A.; Kamal, M. Studies of ionizing radiation shielding effectiveness of silica-based commercial glasses used in Bangladeshi dwellings. *Results Phys.* **2018**, *9*, 541–549. [[CrossRef](#)]
38. Tunes, M.; De Oliveira, C.; Schön, C. Multi-objective optimization of a compact pressurized water nuclear reactor computational model for biological shielding design using innovative materials. *Nucl. Eng. Des.* **2017**, *313*, 20–28. [[CrossRef](#)]
39. Kaewkhao, J.; Pokaipisit, A.; Limsuwan, P. Study on borate glass system containing with Bi_2O_3 and BaO for gamma-rays shielding materials: Comparison with PbO. *J. Nucl. Mater.* **2010**, *399*, 38–40. [[CrossRef](#)]
40. Limkitjaroenporn, P.; Kaewkhao, J.; Limsuwan, P.; Chewpraditkul, W. Physical, optical, structural and gamma-ray shielding properties of lead sodium borate glasses. *J. Phys. Chem. Solids* **2011**, *72*, 245–251. [[CrossRef](#)]
41. Kirdsiri, K.; Kaewkhao, J.; Chanthima, N.; Limsuwan, P. Comparative study of silicate glasses containing Bi_2O_3 , PbO and BaO: Radiation shielding and optical properties. *Ann. Nucl. Energy* **2011**, *38*, 1438–1441. [[CrossRef](#)]
42. Kaewjang, S.; Maghanemi, U.; Kothan, S.; Kim, H.; Limkitjaroenporn, P.; Kaewkhao, J. New gadolinium based glasses for gamma-rays shielding materials. *Nucl. Eng. Des.* **2014**, *280*, 21–26. [[CrossRef](#)]

43. Chanthima, N.; Kaewkhao, J.; Limkitjaroenporn, P.; Tuscharoen, S.; Kothan, S.; Tungjai, M.; Kaewjaeng, S.; Sarachai, S.; Limsuwan, P. Development of BaO–ZnO–B₂O₃ glasses as a radiation shielding material. *Radiat. Phys. Chem.* **2017**, *137*, 72–77. [[CrossRef](#)]
44. Boonin, K.; Yasaka, P.; Limkitjaroenporn, P.; Rajaramakrishna, R.; Askin, A.; Sayyed, M.; Kothan, S.; Kaewkhao, J. Effect of BaO on lead free zinc barium tellurite glass for radiation shielding materials in nuclear application. *J. Non-Crystalline Solids* **2020**, *550*, 120386. [[CrossRef](#)]
45. Cheewasukhanont, W.; Limkitjaroenporn, P.; Kothan, S.; Kedkaew, C.; Kaewkhao, J. The effect of particle size on radiation shielding properties for bismuth borosilicate glass. *Radiat. Phys. Chem.* **2020**, *172*, 108791. [[CrossRef](#)]
46. Kaewjaeng, S.; Kothan, S.; Chaiphaksa, W.; Chanthima, N.; Rajaramakrishna, R.; Kim, H.; Kaewkhao, J. High transparency La₂O₃–CaO–B₂O₃–SiO₂ glass for diagnosis x-rays shielding material application. *Radiat. Phys. Chem.* **2019**, *160*, 41–47. [[CrossRef](#)]
47. ElBatal, F.; Ibrahim, S.; Abdelghany, A. Optical and FTIR spectra of NdF₃-doped borophosphate glasses and effect of gamma irradiation. *J. Mol. Struct.* **2012**, *1030*, 107–112. [[CrossRef](#)]
48. Elbatal, H.; Abdelghany, A.; Elbatal, F.; Elbadry, K.; Moustaffa, F. UV–visible and infrared absorption spectra of gamma irradiated CuO-doped lithium phosphate, lead phosphate and zinc phosphate glasses: A comparative study. *Phys. B Condens. Matter* **2011**, *406*, 3694–3703. [[CrossRef](#)]
49. Gerward, L.; Guilbert, N.; Jensen, K.; Levring, H. WinXCom—a program for calculating X-ray attenuation coefficients. *Radiat. Phys. Chem.* **2004**, *71*, 653–654. [[CrossRef](#)]
50. Tekin, H.O. MCNP-X Monte Carlo Application for Mass Attenuation Coefficients of Concrete at Different Energies by Modeling 3 × 3 Inch NaI(Tl) Detector and Comparison with XCOM and Monte Carlo Data. *Sci. Technol. Nucl. Install.* **2016**, *2016*, 1–7. [[CrossRef](#)]
51. Tekin, H.O.; Singh, V.P.; Manici, T.; Altunsoy, E.E. Validation of MCNPX with Experimental Results of Mass Attenuation Coefficients for Cement, Gypsum and Mixture. *J. Radiat. Prot. Res.* **2017**, *42*, 154–157. [[CrossRef](#)]
52. RSICC Computer Code Collection, MCNPX User’s Manual Version 2.4.0. Monte Carlo N-Particle Transport Code System for Multiple and High Energy Application. 2002. Available online: <https://rsicc.ornl.gov/codes/ccc/ccc8/ccc-810.html> (accessed on 15 January 2021).
53. Şakar, E.; Özpölat, Ö.F.; Alım, B.; Sayyed, M.; Kurudirek, M. Phy-X/PSD: Development of a user friendly online software for calculation of parameters relevant to radiation shielding and dosimetry. *Radiat. Phys. Chem.* **2020**, *166*, 108496. [[CrossRef](#)]
54. Bashter, I. Calculation of radiation attenuation coefficients for shielding concretes. *Ann. Nucl. Energy* **1997**, *24*, 1389–1401. [[CrossRef](#)]
55. Issa, S.A.; Saddeek, Y.B.; Tekin, H.; Sayyed, M.; Shaaban, K.S. Investigations of radiation shielding using Monte Carlo method and elastic properties of PbO–SiO₂–B₂O₃–Na₂O glasses. *Curr. Appl. Phys.* **2018**, *18*, 717–727. [[CrossRef](#)]